Electronic Supplementary Material (ESI) for Journal of Materials Chemistry A.

Electronic Supplementary Information (ESI)

Self-assembly of Polyoxometalate / Reduced Graphene Oxide Composites Induced by Ionic Liquids as High Rate Cathode for Batteries: Killing Two Birds with One Stone

Feng-Cui Shen[a,b,c], Yi-Rong Wang[b], Shun-Li Li[b], Jiang Liu[b], Long-Zhang Dong[b], Tao Wei[b], Xing Long Wu[d], Yan Xu and Ya-Qian Lan[b]**

[a] *College of Chemical Engineering, State Key Laboratory of Materials-Oriented Chemical Engineering, Nanjing Tech University, Nanjing 210009, P. R. China*

[b] *Jiangsu Collaborative Innovation Centre of Biomedical Functional Materials, Jiangsu Key Laboratory of New Power Batteries, School of Chemistry and Materials Science, Nanjing Normal University, Nanjing 210023, China*

[c] *School of Biological and Chemical Engineering, Anhui Polytechnic University, Wuhu, 241000, P. R. China*

[d] *National and Local United Engineering Laboratory for Power Batteries. Faculty of Chemistry Northeast Normal University, Changchun, Jilin 130024, P. R. China*

*Correspondence to: yqlan@njnu.edu.cn

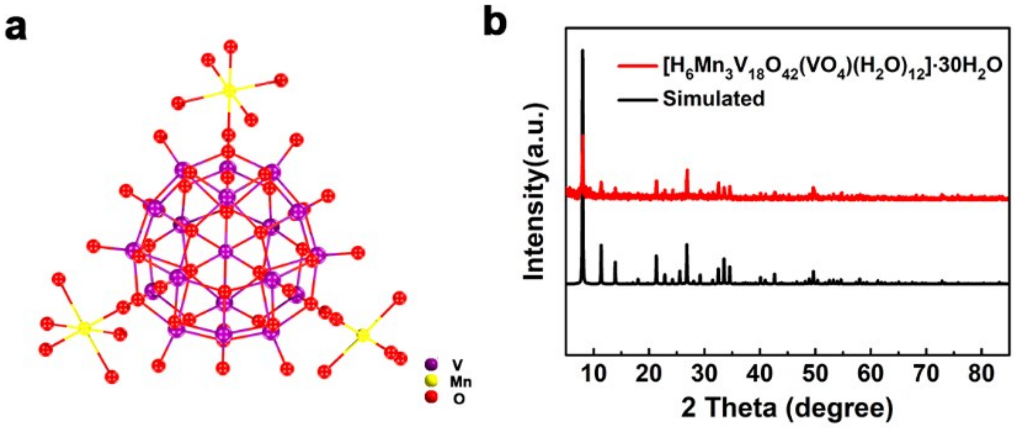

Figure S1. View of the crystal structure and corresponding XRD characterization of $[H_6Mn_3V_{18}O_{42}(VO_4)\ (H_2O)_{12}]\ 30H_2O$. (a) crystal structure of $[H_6Mn_3V_{18}O_{42}(VO_4)\ (H_2O)_{12}]$ $30H_2O$. (b) corresponding XRD pattern, the simulated XRD was obtained by Single-crystal X-ray diffraction analysis.

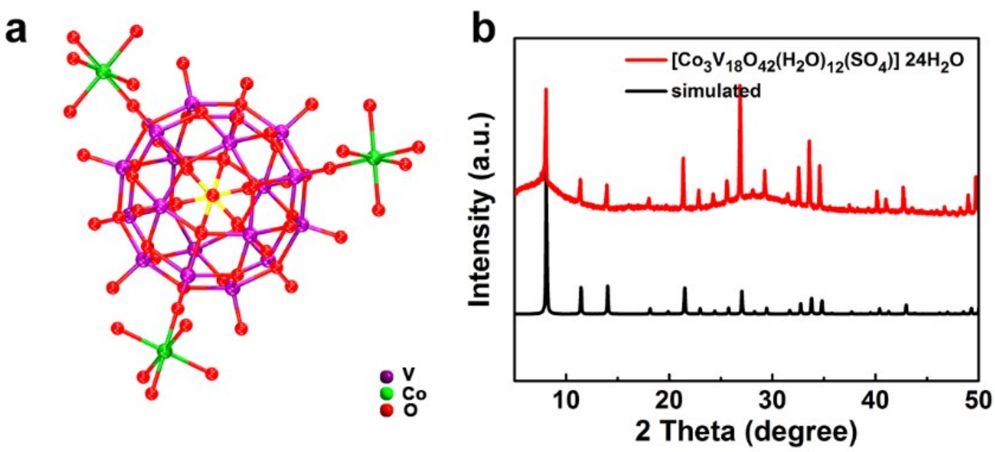

Figure S2. View of the crystal structure and corresponding XRD characterization of $Co_3V_{18}O_{42}(H_2O)_{12}(SO_4)\ 24H_2O$. (a) crystal structure $Co_3V_{18}O_{42}(H_2O)_{12}(SO_4)\ 24H_2O$. (b) corresponding XRD pattern, the simulated XRD was obtained by Single-crystal X-ray diffraction analysis.

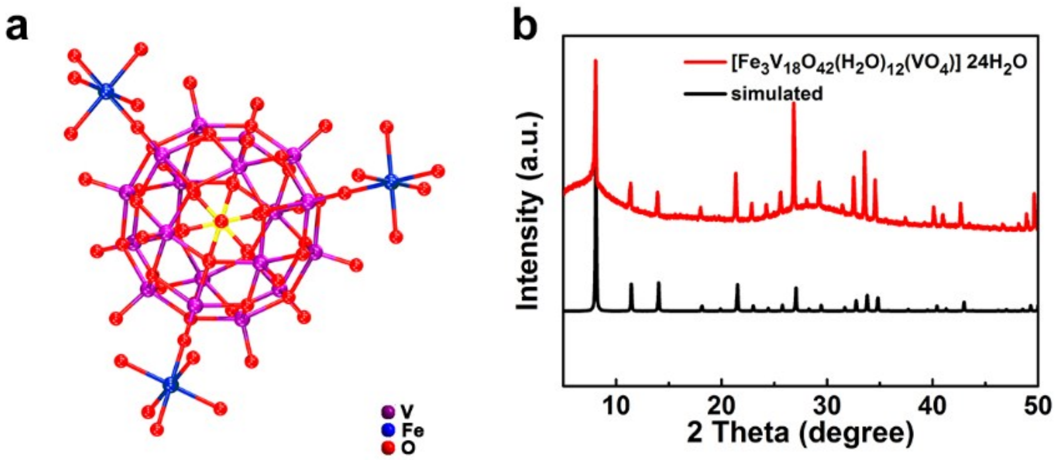

Figure S3. View of the crystal structure and corresponding XRD characterization of $Fe_3V_{18}O_{42}(H_2O)_{12}(VO_4)$ $24H_2O$. (a) crystal structure $Fe_3V_{18}O_{42}(H_2O)_{12}(VO_4)$ $24H_2O$. (b) corresponding XRD pattern, the simulated XRD was obtained by Single-crystal X-ray diffraction analysis.

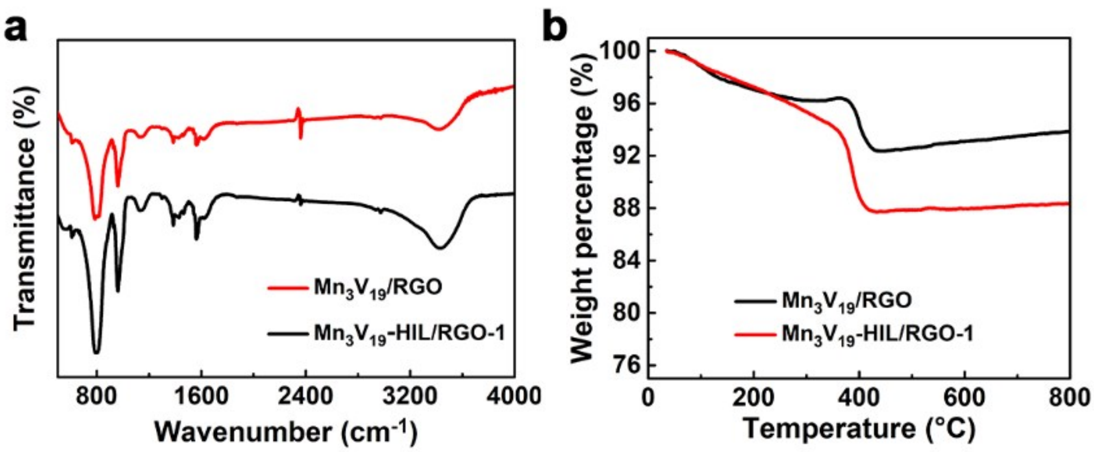

Figure S4. FT-IR and TG characterization of composites. (a) Infrared Spectroscopy and (b) TG curve of Mn_3V_{19}/RGO and Mn_3V_{19}-HIL/RGO-1.

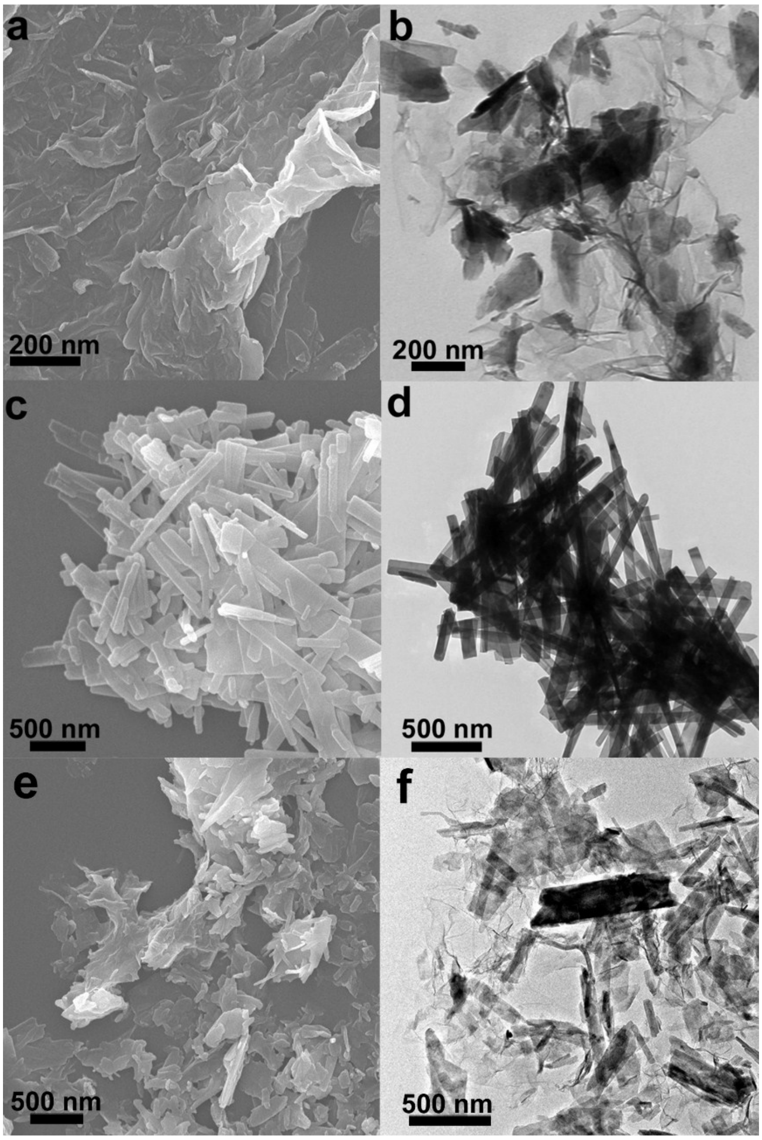

Figure S5. SEM and TEM images of relative composites. (a) SEM and (b) TEM image of Mn_3V_{19}/RGO, (c) SEM and (d) TEM image of Mn_3V_{19}-HIL, (e) SEM and (f) TEM image of Mn_3V_{19}-EIL/RGO synthesized.

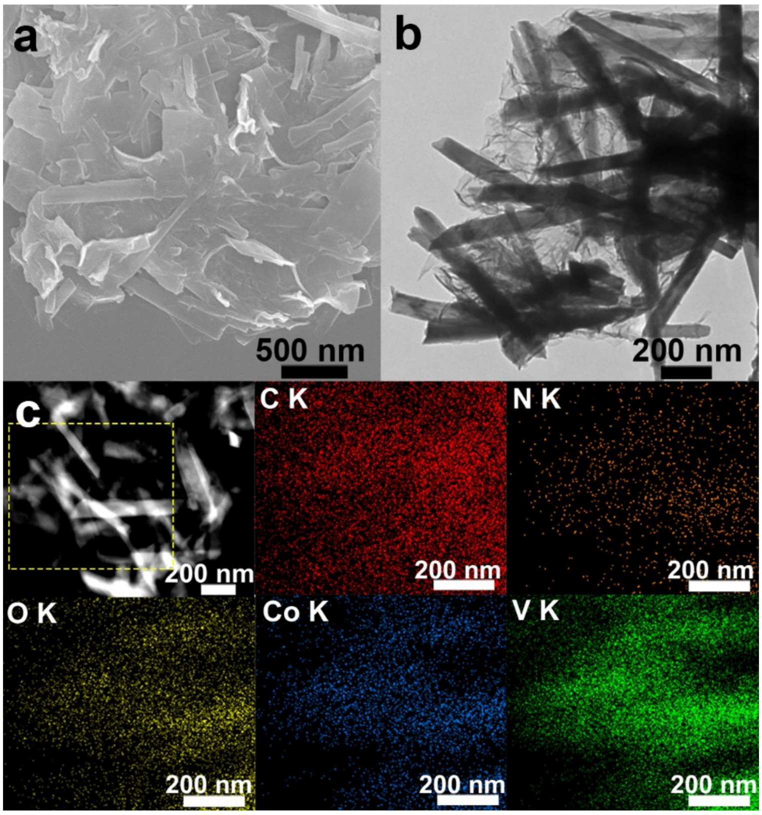

Figure S6. The morphology characterization of Co_3V_{18}-HIL/RGO. (a) SEM, (b) TEM image and (c) corresponding mappings of Co_3V_{18}-HIL/RGO synthesized.

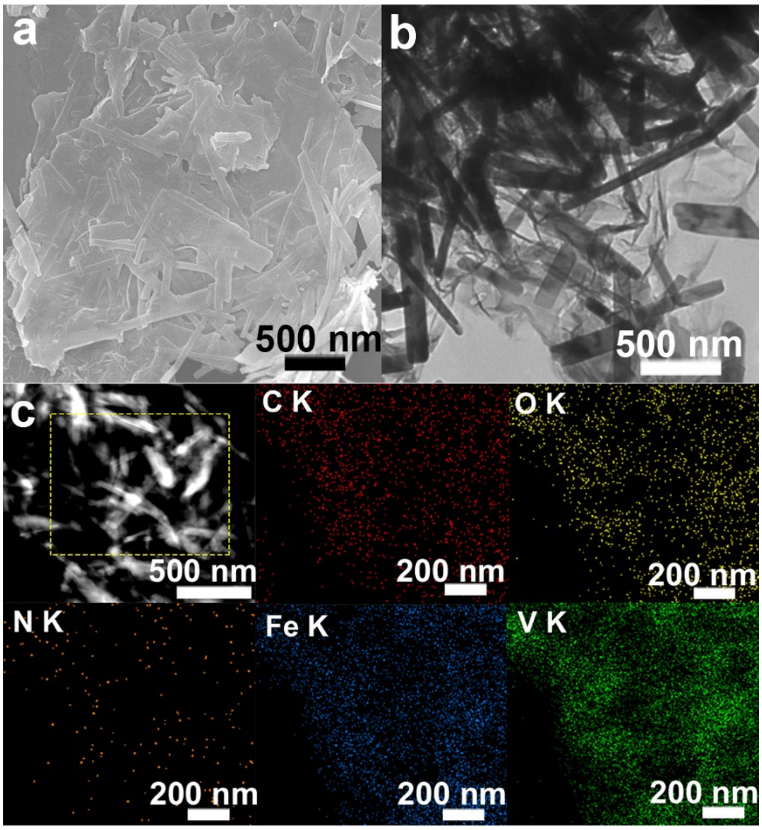

Figure S7. The morphology characterization of Fe_3V_{19}-HIL/RGO. (a) SEM, (b) TEM image and (c) corresponding mappings of Fe_3V_{19}-HIL/RGO synthesized.

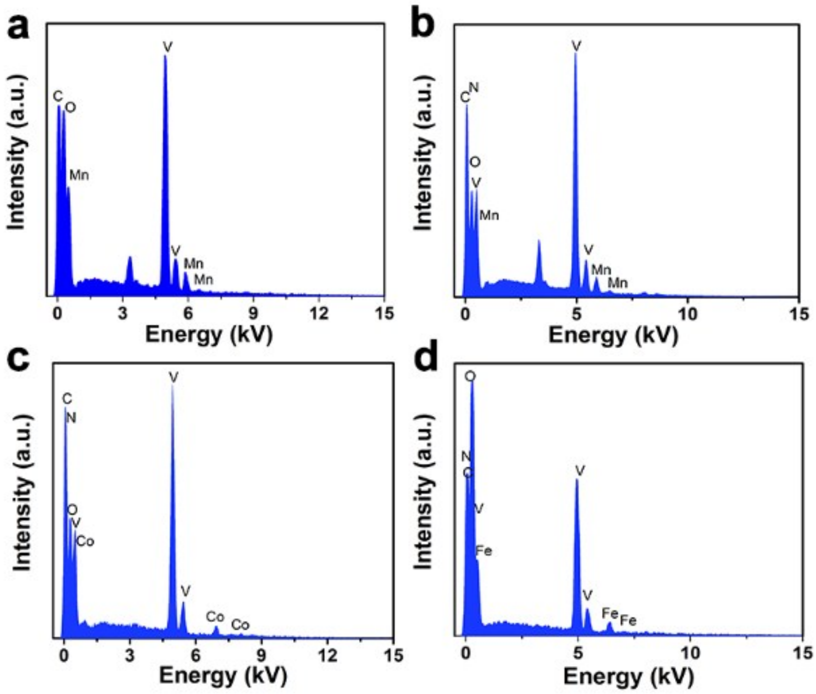

Figure S8. EDS analysis. EDS spectrum of (a) Mn_3V_{19}/RGO, (b) Mn_3V_{19}-HIL/RGO-1, (c) Co_3V_{18}-HIL/RGO and (d) Fe_3V_{19}-HIL/RGO composite.

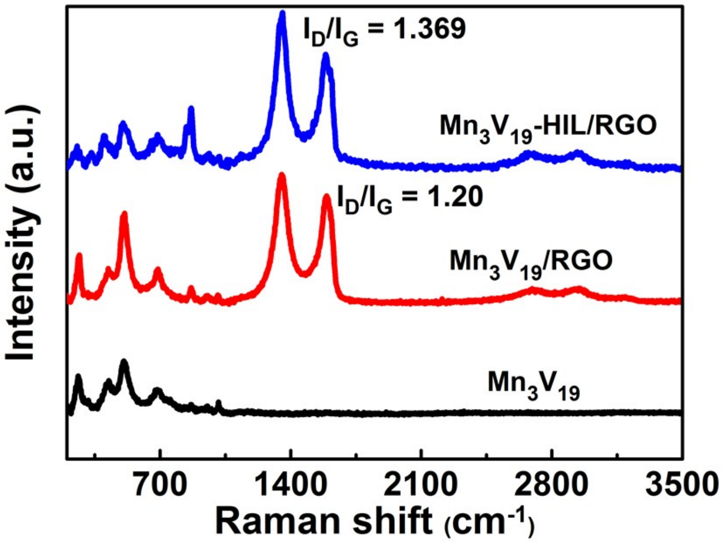

Figure S9. Raman spectra of Mn_3V_{19}, Mn_3V_{19}/RGO and Mn_3V_{19}-HIL/RGO-1.

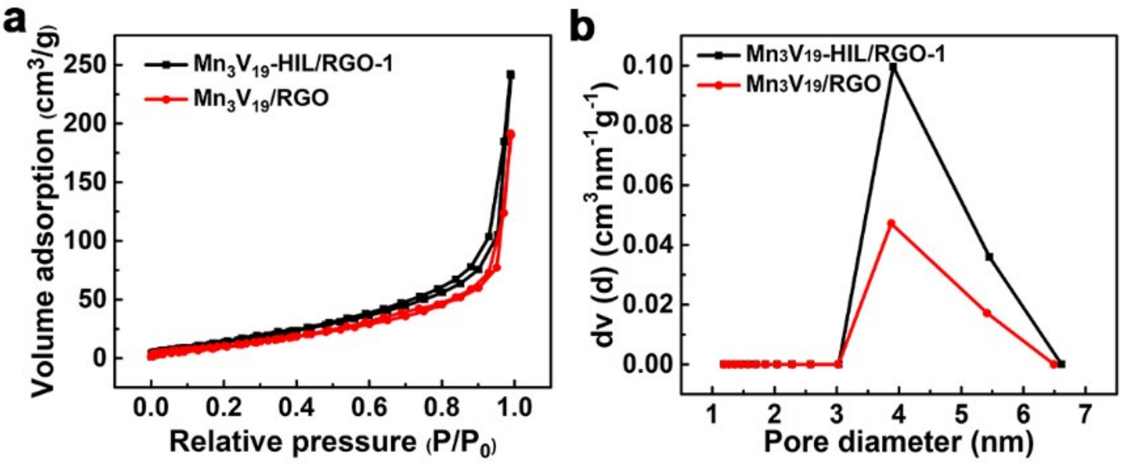

Figure S10. N_2 adsorption-desorption isotherm and pore size distribution. (A) Nitrogen adsorption-desorption isotherms of Mn_3V_{19}/RGO and Mn_3V_{19}-HIL/RGO-1 respectively. (B) The pore size distribution of the samples by BJH method.

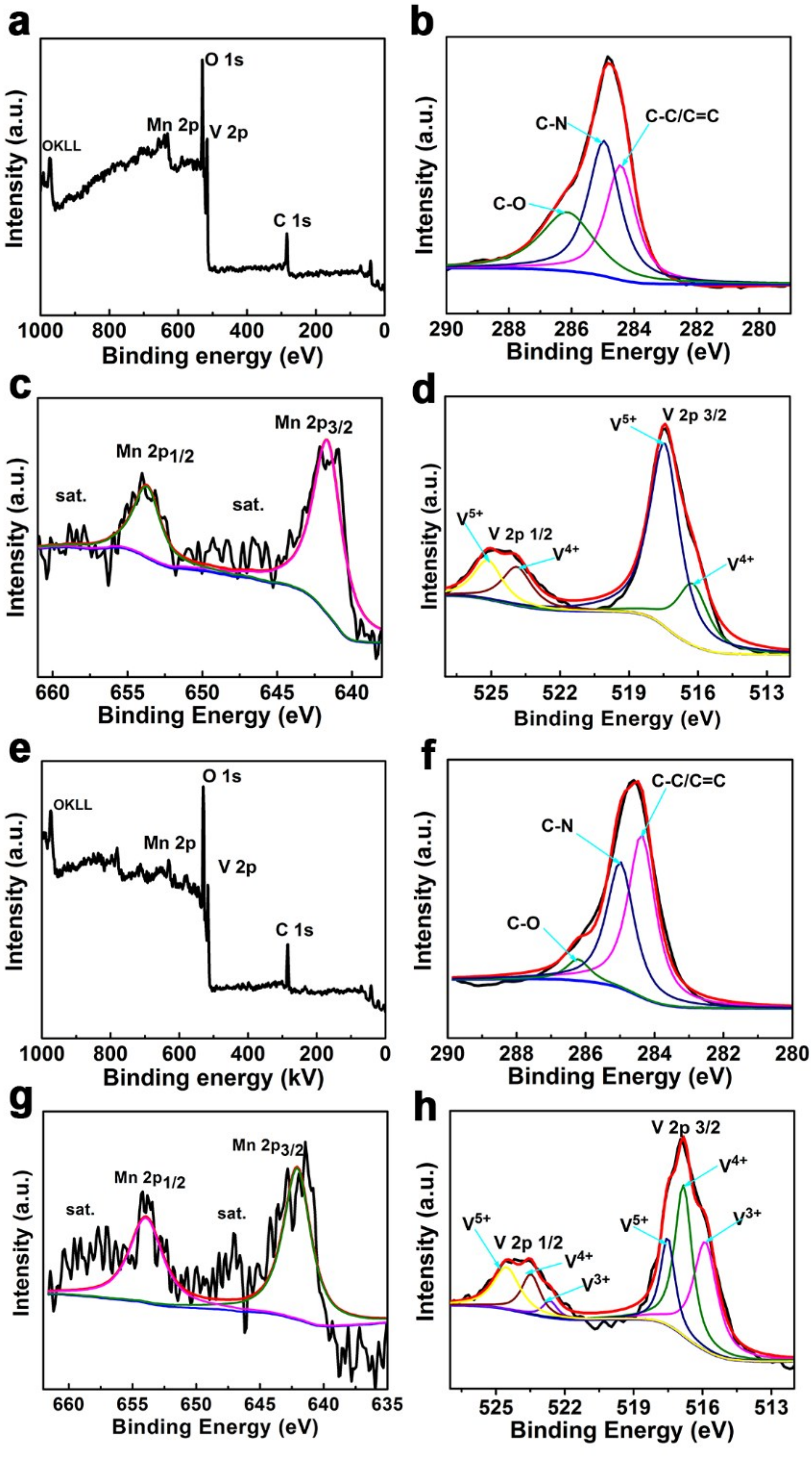

Figure S11. XPS analysis. High-resolution XPS spectra of the Mn_3V_{19}-HIL/RGO-1 at the lithiated (a-d) and delithiated state (e-h) of LIBs.

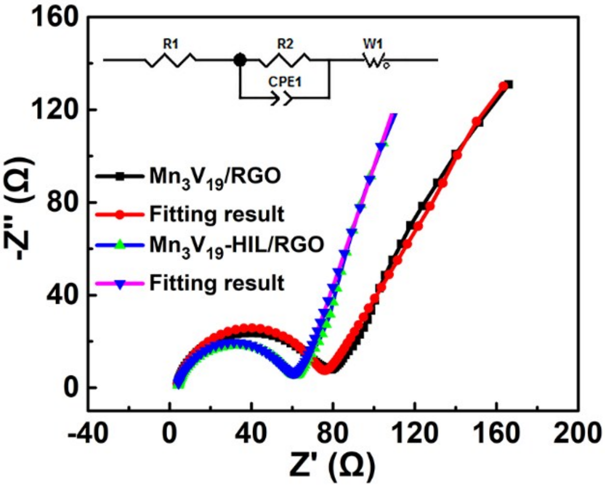

Figure S12. Nyquist plots of Mn_3V_{19}-HIL/RGO-1 and Mn_3V_{19}/RGO-1 electrodes in LIBs.

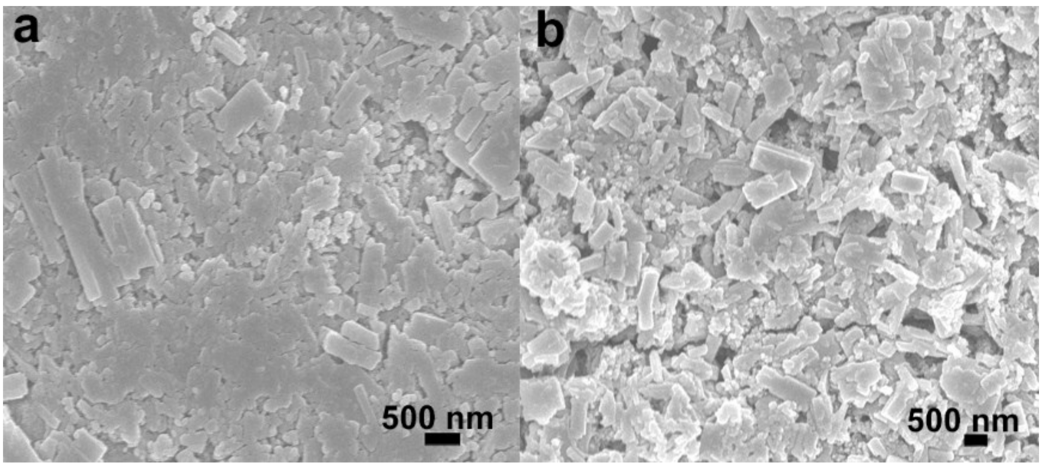

Figure S13. SEM images of the Mn_3V_{19}-HIL/RGO-1 electrode. (a) before and (b) after cycles in LIBs.

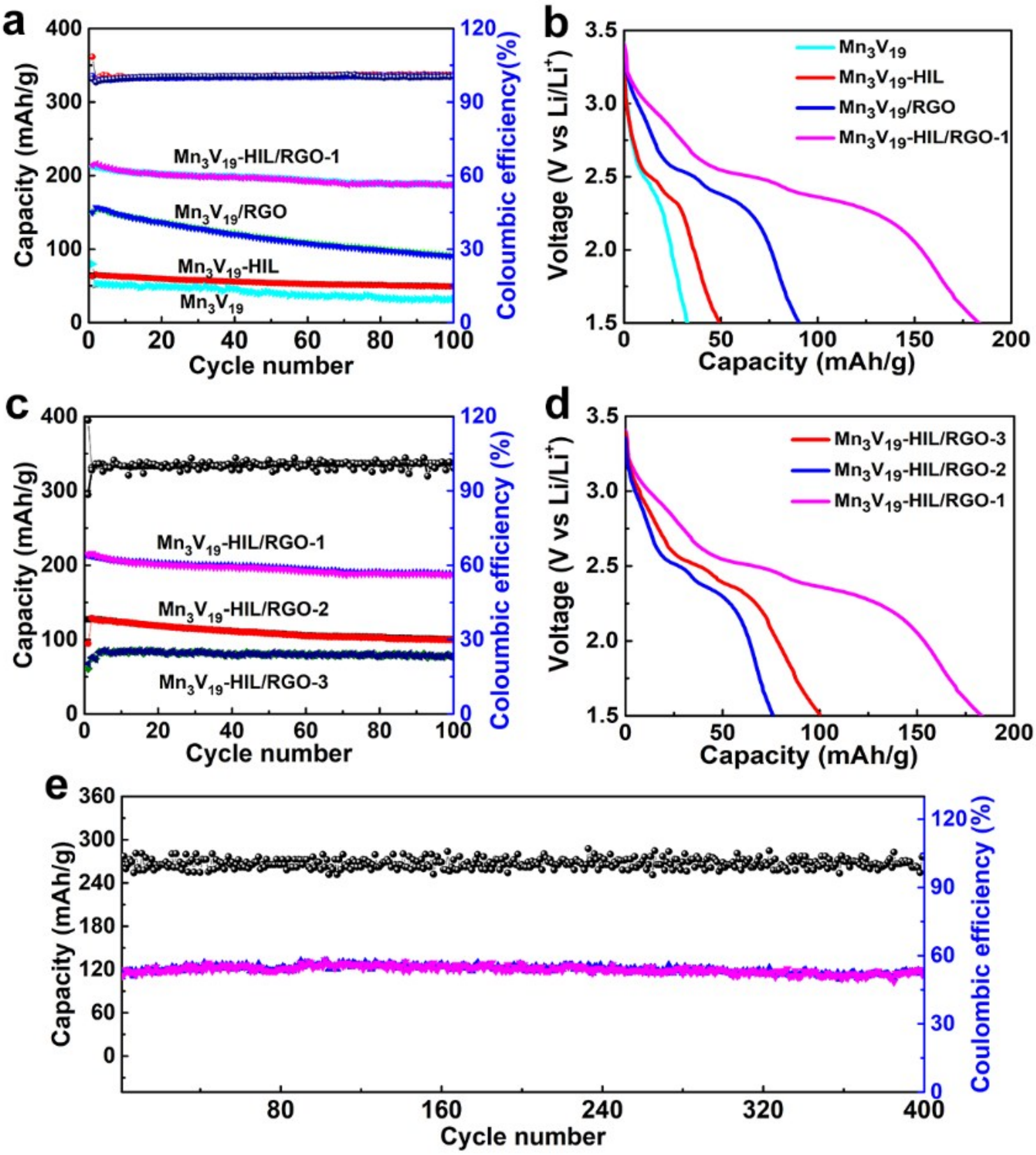

Figure S14. Electrochemical characterization of Mn_3V_{19}-HIL/RGO relative composites as LIB cathodes. (a) Cycle stability of Mn_3V_{19}-HIL/RGO-1, Mn_3V_{19}/RGO and Mn_3V_{19}-HIL at 100 mA g^{-1} and (b) the corresponding discharge curves of 100th cycles. (c) Cycle stability of Mn_3V_{19}-HIL/RGO-1, Mn_3V_{19}-HIL/RGO-2 and Mn_3V_{19}-HIL/RGO-3 and (d) the corresponding discharge curves of 100th cycles. (e) Cycling performance of Mn_3V_{19}-HIL/RGO-1 at 5 A/g.

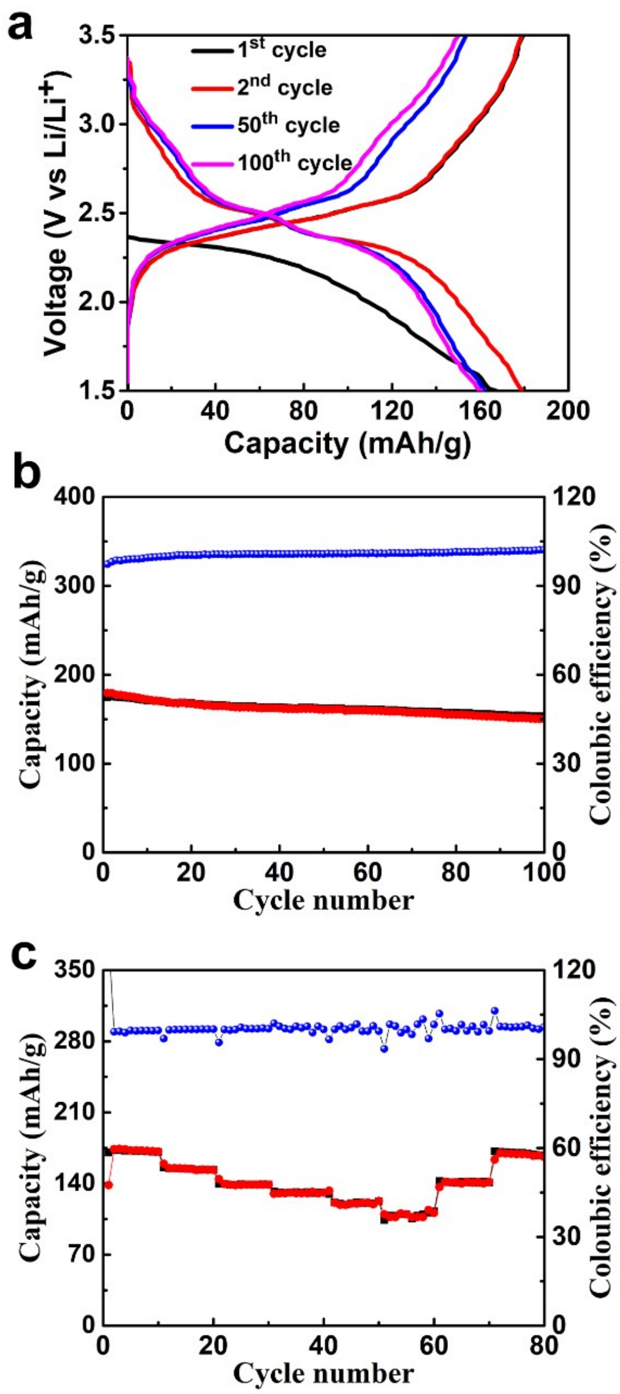

Figure S15. Electrochemical characterization of Mn_3V_{19}-EIL/RGO as the LIB cathode. (a) Discharge–charge curves of Mn_3V_{19}-EIL/RGO at 100 mA g^{-1}. (b) Cycle stability of Mn_3V_{19}-EIL/RGO at 100 mA g^{-1}. (c) Rate capability performance of Mn_3V_{19}-EIL/RGO at various current densities (100, 200, 400, 1000, 2000, 5000, 1000, 100 mA g^{-1}).

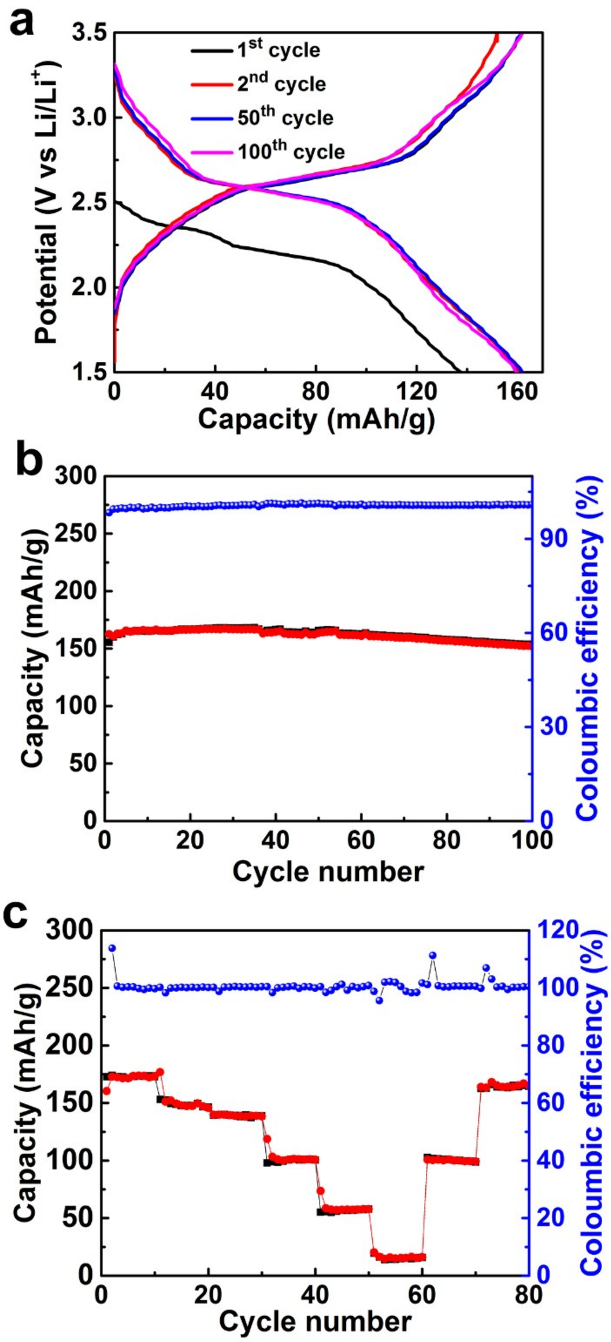

Figure S16. Electrochemical characterization of Co_3V_{18}-HIL/RGO as the LIB cathode. (a) Discharge–charge curves and (b) Cycle stability of Co_3V_{18}-HIL/RGO at 100 mA g^{-1}. (c) Rate capability performance of Co_3V_{18}-HIL/RGO at various current densities (100, 200, 400, 1000, 2000, 5000, 1000, 100 mA g^{-1}).

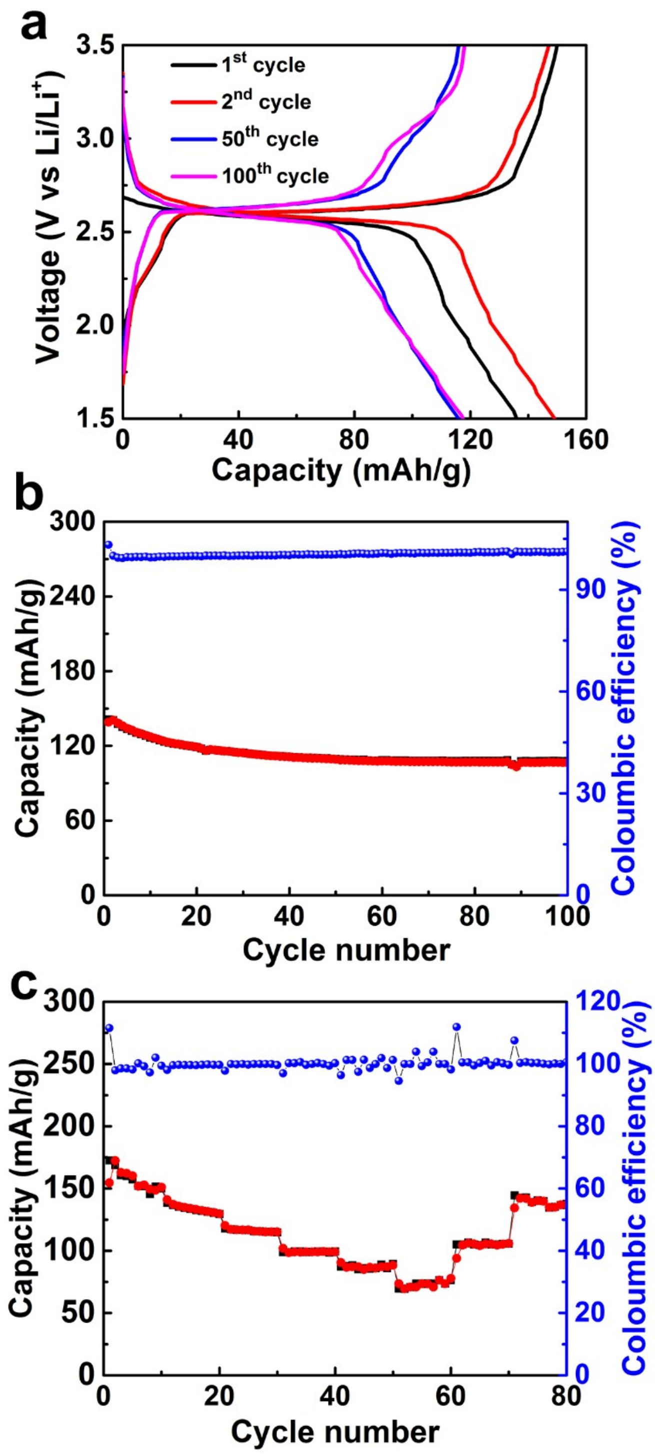

Figure S17. Electrochemical characterization of Fe_3V_{19}-HIL/RGO as the LIB cathode. (a) Discharge–charge curves and (b) Cycle stability of Fe_3V_{19}-HIL/RGO at 100 mA g^{-1}. (c) Rate capability performance of Fe_3V_{19}-HIL/RGO at various current densities (100, 200, 400, 1000, 2000, 5000, 1000, 100 mA g^{-1}).

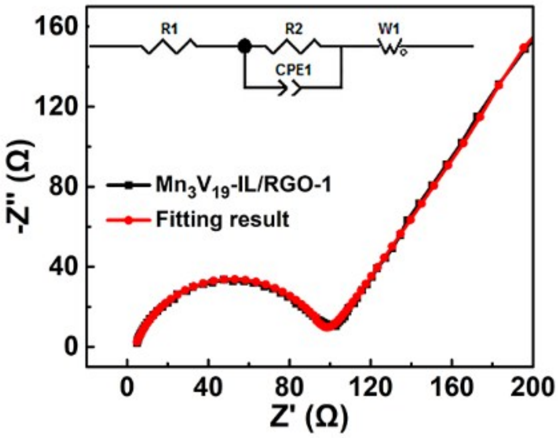

Figure S18. Nyquist plots of Mn_3V_{19}-HIL/RGO-1 electrodes in SIBs.

Supplemental Tables

Table S1. Ratio of the elements in Mn_3V_{19}-HIL/RGO-1, Co_3V_{18}-HIL/RGO and Fe_3V_{19}-HIL/RGO cathode.

element	C	N	O	Mn	V
atomic percent (%)	39.25	3.72	39.01	2.3	15.71
element	C	N	O	Fe	V
atomic percent (%)	24.2	4.64	48.64	2.14	20.38
element	C	N	O	Co	V
atomic percent (%)	21.95	5.46	49.44	1.78	21.37

Table S2. Comparison of relevant cathode for SIBs.

Cathode composite	RC (mAh g^{-1})/ CR(mAh g^{-1})	HRC (mAh g^{-1})/ CR(mAh g^{-1})	Potential range (V)	Active material ratio(%)	Ref
Mn_3V_{19}-HIL/RGO-1	156.3/100 (50 cycles)	92/500 (200 cycles)	1.5-3.5	70	This work
Na2H8[MnV13O38]/G	140/26 (0.2C) (100 cycle)	～75/420	1.5-3.9	70	1
$K_3V_2(PO_4)_3$/C	119/100 (100 cycles)	～62/500 (1000 cycles)	1.5-4	50	2
R-Na2−δMnHFC	～105/100 (100 cycles)	120/1850 (20C)	2-4	70	3
$Na_2Mn^{I}[Mn^{II}(CN)_6]$	～209/40 (frist cycles)	～130/400 (2C) (100 cycles)	1.2-4	80	4
P2-$Na_{0.7}CoO_2$	125/5 (5 cycles)	～95/50 (0.4C) (300 cycles)	2-3.8	70	5
PDMS/rGO sponge/$VOPO_4$	～126/50 (five cycles)	～85/400 (300 cycles)	2.5–4.3	80	6

RC: Reversible capacity. CR: Charge rate.

Table S3. Comparison of relevant cathode for LIBs.

Cathode composite	RC (mAh g^{-1})/ CR(mAh g^{-1})	RC (mAh g^{-1})/ CR(mAh g^{-1})	Potential range (V)	Active material ratio(%)	Ref
Mn_3V_{19}-HIL/RGO-1	188.1/100 (100 cycles)	121/5000 (400 cycles)	1.5-3.5	70	This work
$Li_7[V_{15}O_{36}(CO_3)]$	250/50 (the first cycle)	150/2000 (100 cycles)	1.9-4	70	7
PANI/PMo_{12}	149.5/27 (50 cycles)	～100/540 (5 cycles)	1.5-4.2	75	8
SiW_{12}/rGO	～160/10 (10 cycles)	120/2000 (10 cycles)	1.5-4	60	9
VS_2/GNS	185.3/36 (200 cycles)	114/3600 (5 cycles)	1.5−3.5	70	10
3S-V_2O_5-HMSs	402.4/1000 (100 cycles)	331.8/2000 (11 cycles)	1.5-4.0	70	11
HNS VO_2	134/100 (100 cycles)	105.3/1000 (500 cycles)	2-3	70	12
$LiMn_2O_4$ CSC-NPs	122/121 (5 cycles)	99/2420 (400 cycles)	3-4.5	65	13
TiO_2 microboxes	187/170 (300 cycles)	63/3400 (20 cycles)	1-3	70	14

RC: Reversible capacity. CR: Charge rate.

Reference

1. J. Liu, Z. Chen, W. Xuan, S. Chen, B. Zhang, J. Wang, H. Wang, B. Tian, M. Chen, X. Fan, Y. Huang, T. C. Sum, J. Lin and Z. X. Shen, *ACS Nano*, 2017, **11**, 6911-6920.
2. X. Wang, C. Niu, J. Meng, P. Hu, X. Xu, X. Wei, L. Zhou, K. Zhao, W. Luo, M. Yan and L. Mai, *Adv. Energy Mater.*, 2015, **5**, 1500716.
3. J. Song, L. Wang, Y. Lu, J. Liu, B. Guo, P. Xiao, J.-J. Lee, X.-Q. Yang, G. Henkelman and J. B. Goodenough, *J. Am. Chem. Soc.* , 2015, **137**, 2658-2664.
4. H.-W. Lee, R. Y. Wang, M. Pasta, S. Woo Lee, N. Liu and Y. Cui, 2014, **5**, 5280.
5. Y. Fang, X.-Y. Yu and X. W. Lou, *Angewandte Chemie*, 2017, **129**, 5895-5899.
6. H. Li, Y. Ding, H. Ha, Y. Shi, L. Peng, X. Zhang, C. J. Ellison and G. Yu, *Adv. Mater.* , 2017, **29**, 1700898.
7. J. J. Chen, M. D. Symes, S. C. Fan, M. S. Zheng, H. N. Miras, Q. F. Dong and L. Cronin, *Adv. Mater.*, 2015, **27**, 4649-4654.
8. H. Yang, T. Song, L. Liu, A. Devadoss, F. Xia, H. Han, H. Park, W. Sigmund, K. Kwon and U. Paik, *The Journal of Physical Chemistry C*, 2013, **117**, 17376-17381.
9. S. Wang, H. Li, S. Li, F. Liu, D. Wu, X. Feng and L. Wu, *Chemistry – A European Journal*, 2013, **19**, 10895-10902.
10. W. Fang, H. Zhao, Y. Xie, J. Fang, J. Xu and Z. Chen, *ACS Appl. Mat. Interfaces* 2015, **7**, 13044-13052.
11. J. Wang, H. Tang, L. Zhang, H. Ren, R. Yu, Q. Jin, J. Qi, D. Mao, M. Yang, Y. Wang, P. Liu, Y. Zhang, Y. Wen, L. Gu, G. Ma, Z. Su, Z. Tang, H. Zhao and D. Wang, *Nat. Energy*, 2016, **1**, 16050.
12. L. Mai, Q. Wei, Q. An, X. Tian, Y. Zhao, X. Xu, L. Xu, L. Chang and Q. Zhang, *Adv. Mater.* , 2013, **25**, 2969-2973.
13. S. Lee, Y. Cho, H.-K. Song, K. T. Lee and J. Cho, *Angew. Chem. Int. Ed.* , 2012, **51**, 8748-8752.
14. X. Gao, G. Li, Y. Xu, Z. Hong, C. Liang and Z. Lin, *Angew. Chem. Int. Ed.* , 2015, **54**, 14331-14335.